# Nanoparticles embedded in a sponge of polydimethylsiloxane by laser ablation in liquid

*Mariapompea Cutroneo*[1*], *Vladimir* Havranek[1], *Lorenzo* Torrisi[2], *Letteria* Silipigni[2], *Lubomir* Kovacik[3], *Petr* Malinsky[1,4], *Josef* Flaks[1], *Petr* Slepicka[5], *Dominik* Fajstavr[5], *Olga* Janoušková[6], *Daniela* Zbořilová[6] and *Anna* Mackova[1,4]

[1]Nuclear Physics Institute, AS CR, 25068 Rez, Czech Republic
[2]Department of Physics (MIFT), Messina University, V. le F.S. d'Alcontres 31, 98166 S. Agata, Messina, Italy
[3]Center for Cellular Imaging and NanoAnalytics (C-CINA) Biozentrum, University of Basel, CH-4058 Basel, Switzerland
[4]Department of Physics, Faculty of Science, University of J. E. Purkyně, Pasteurova 3544/1, 400 96 Ústí nad Labem, Czech Republic
[5]Department of Solid State Engineering, Institute of Chemical Technology, 166 28 Prague, Czech Republic
[6] Department of Biology, Faculty of Science, University of J. E. Purkyně, Pasteurova 15, 400 96 Ústí nad Labem, Czech Republic

**Abstract.** This work describes the preparation of polydimethylsiloxane (PDMS) sponge with pore sizes of about 50 and 900 µm. The sponges synthetized by the sugar template process were embedded with graphene oxide (GO) and gold nanoparticles (AuNPs) previously produced by laser ablation in liquid. The suspension containing graphene oxide and gold nanoparticles were optically characterized by UV-ViS spectroscopy. The dispersion of the nanoparticles in the PDMS sponges was observed by the Scanning Electron Microscopy (SEM). The biocompatibility of virgin PDMS, PDMS filled with graphene oxide, and with graphene oxide and gold nanoparticles was studied for different types of cell cultures. This study has allowed us to confirm that the PDMS sponge is a good matrix for embedding AuNPs and has highlighted as the presence of GO hinders the aggregation of AuNPs avoiding the use of surfactant and allowing their use in biological applications.

## 1 Introduction

Polymer composites have recently attracted intensive research interest in nanoelectronics, polymeric bionanomaterials, nanocomposite-based drug delivery systems, etc. The loading of fillers in polymers can produce a significant improvement in mechanical, thermal, electrical, optical, properties. The functionalization of the polymer obtained by incorporating nanoparticles (NPs), is correlated to the NPs homogeneous distribution and

* Corresponding author: cutroneo@ujf.cas.cz

dispersion. In this frame, the use of porous 3D material appears promising for larger surface area-to-volume ratio, easier mixing of filler whatever the wettability of the native polymer is, better anchoring of filler and synthesis of the final material. In our previous papers **[1]** polydimethylsiloxane (PDMS) sponges with porosity of 50-900 μm were produced for applications in biomedicine **[2]**. PDMS is an elastomer containing the Si-O-Si backbone which is responsible for its flexibility, handling, electrical resistance **[3]**. Further characteristics making PDMS promising for biomedical applications such as cell-based implants are represented by: chemical inertness, oxygen permeability, thermal stability, mechanical resistance. The desired structural, surface and functional modifications of the PDMS are explicitly related to the type, amount and choice of fillers. Metals **[4]**, nanoclays, carbon nanotubes and graphene are mostly applied for improving strength, antimicrobial resistance, adhesion, electrical and thermal conductivity, multi-cyclic deformations, stress endurance for advances in polymer composites. The presence of gold nanoparticles (Au NPs) is evinced when an incident light beam is strongly absorbed by the nanostructures at characteristic wavelength bands. This is a consequence of the coupling of the electric field of the incident light to the electric-field induced dipolar oscillations of the valence electrons on the surface of metallic NPs **[5]**.

Another promising nanosized material used as filler, is graphene oxide (GO). It is a single layer of graphite with the epoxide and hydroxyl groups at the basal plane and the carbonyl and carboxyl groups at the edges. The physical properties of GO depend on the $sp^2$ to $sp^3$ hybridized carbon atoms ratio and on the different functional groups. The native insulating nature of GO can be turned in more conductive reduced graphene oxide (rGO) **[6]** by thermal treatment, laser irradiation, electron and ion irradiation **[7]**. Graphene oxide has been used as antimicrobial agent for the water disinfection to remove organic molecules and waterborne pathogens **[8]**, radiation sensitive material **[9]**, dosimeter **[10]** and sensors **[11]**.

In this work, nanoparticles are produced by laser ablation in medium by monitoring the laser fluence, the laser wavelength, the irradiation time and the type of employed liquid **[12]**. The laser beam, focused on the surface of a solid target placed in a vessel containing a liquid, generates a plasma plume at the solid-liquid interface. This last expands due to the reaction occurring inside and a vapor layer is formed. The vapor layer expands into a cavitation bubble while the plasma plume shrinks because of the compression provoked by the vapor layer and then collapses. Nanoparticles are released first in the cavitation bubble and after its collapsing into water. Nanoparticles stop to grow when they reach the same temperature as the water **[13].**

In particular, in the present study, porous polydimethylsiloxane **[1]**, embedded with gold nanoparticles and gold nanoparticles anchored to graphene oxide, is obtained. Both nanoparticles are produced by laser ablation in liquid and the validity of the method for the preparation of composites for biomedical applications will be reported.

## 2 Materials and Methods

### 2.1 Preparation of gold nanoparticles by laser ablation

A nanosecond Nd:YAG Litron laser **[14]** operating at 1064 nm, 4 ns pulse duration, 375 mJ pulse energy, in the 2.5 Hz repetition mode, was employed to irradiate a solid target of gold (99.99 % purity, Goodfellow). The laser beam was directed to a quartz prism and focused by a lens, with a 50 cm focal length, on the Au target placed in a beaker vessel containing 5 ml of liquid. The used setup for the nanoparticle synthesis is shown in **Fig. 1**. Two liquids have been used: 5 ml of distilled water for the production of Au+$H_2O$ and 0.5 ml of GO mixed with 4.5 ml of distilled water for the production of GO+Au+$H_2O$. The concentration of

produced Au NPs was evaluated by weighing the gold target before and after 5 minutes of laser ablation and calculating its weight loss. In accordance with RBS and EDX analyses reported in the following sections, it is reasonable to assume that Au NPs have spherical shape with average diameter of about 10 nm as confirmed by SEM and optical analyses and same density as bulk gold (i.e. 19.3 g/cm$^3$). The Au NPs concentration was calculated to be 1.0 x $10^{14}$ NPs/cm$^3$ in Au +$H_2O$ and 1.9 x $10^{13}$ NPs/ cm$^3$ in GO+Au+$H_2O$. The PDMS (Sylgard 184 Dow Corning) was obtained mixing the prepolymer (monomer) and the curing agent (crosslinker) in a 1:10 weight ratio.

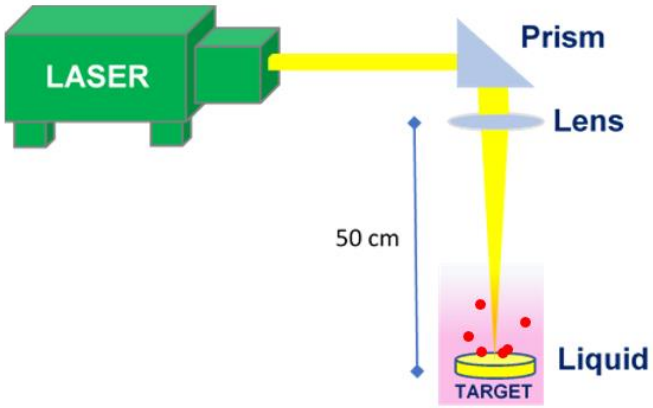


**Fig. 1.** Sketch of the laser set-up for the synthesis of nanoparticles by laser ablation in medium.

The PDMS solution was placed in a glass beaker containing four sugar bricks (about 1 cm$^3$ in size) in a vacuum chamber to improve the gassing and the capillarity infiltration of the solution into the hollows of the sugar bricks **[15]**. Successively the sugar bricks filled with the PDMS, were thermally cured in an oven for 45 minutes at 100° C in air. The obtained PDMS sponges were immersed in deionized water at 60° C to completely dissolve the sugar powders and dried in air. Over the four PDMS sponges, three were immersed in glass beakers containing 1.1 g of GO+ $H_2O$, GO+ Au+$H_2O$ and Au+ $H_2O$ suspensions while the last one was used as virgin for comparison during the following characterization investigations.

## 2.2 Rutherford backscattering spectrometry (RBS)

The compositional changes of the solutions during the laser irradiation were monitored by Rutherford backscattering spectrometry (RBS). Each one of the three suspensions with a volume of 0.5 ml was poured on silicon substrates and then dried in air. To reduce the background and avoid the generation of resonances in Si during the RBS analysis, a proton beam of 1.3 MeV was chosen. The ion current was 2.2 nA and the beam spot size was (1.8x1.8) mm$^2$. The backscattered ions were monitored by an Ultra-Ortec PIPS silicon detector located at a 160° scattering angle. RBS energy scale spectra were converted in concentration depth profile using the SIMNRA simulation code **[16].** The energy loss of protons in the investigated materials has been evaluated using the SRIM code **[17].**

### 2.3 UV-Vis spectroscopy

The optical transmittance **[18]** of the suspensions was acquired in the wavelength interval ranging between 300 nm and 700 nm using an AvaSpec-2048 spectrometer with a UB-600 lines/mm grating. The light generated by a halogen-deuterium dual source, illuminated at 0° the front side of the quartz cuvette containing a suspension while the probe connected to the spectrometer was placed behind the cuvette at 180° in the transmission configuration.

### 2.4 Scanning Electron Microscopy (SEM)

The morphology of the produced nanoparticles in the three suspensions was studied by a TESCAN LYRA3 GMU (Tescan, CZ) system in the secondary-electron mode using an acceleration voltage of 5 kV. The view fields of the probed surfaces were 20 μm, 5 μm and 2 μm for a better identification of the nanoparticles. Being SEM equipped with an Energy Dispersive X-ray spectrocopy (EDX) probe it has been also possible to perform X-ray fluorescence microanalysis induced by (5÷20) keV electron beams on the investigated samples.

### 2.5 Cytotoxicity analysis

The cytotoxicity analysis was performed using two cancer cell line (human mammary carcinoma cell line-MCF7 and human prostat carcinoma cell line-PC3) and one primary cell line (rat mesenchymal cells – rMSC). The cells were incubated with PDMS composites for 72 hours then the PrestoBlue cell viability assay were used to quantify viability of cells. PrestoBlue is cell permeable resazurin-based solution that functions as a cell viability indicator by using the reducing power of living cells to quantitatively measure the proliferation of cells. Resazurin in living cells is modified by the reducing environment of the viable cell and turns red in colour, becoming highly fluorescent. This color change can be detected using fluorescence or absorbance measurements. Table I lists the types of culture cells as well as the cell media.

**Table I** - Cell lines, morphology and culture medium of three different culture cells used for cytotoxicity analysis

| CELL LINE | PROVENIENCE | MORPHOLOGY | CULTURE MEDIUM |
|---|---|---|---|
| **MCF7** | human breast/mammary adenocarcinoma | epithelial-like | EMEM |
| **PC3** | human prostate adenocarcinoma | epithelial | DMEM/F12 |
| **rMSC** | rat mesenchymal stem cells | stromal | DMEM |

The description of the assay: The cells, $2x10^4$ in 1 ml of cultivation media, were seeded into individual wells of a 24-well plate the day before the addition of prepared samples. The piece of prepared sponge ($2x3\text{-}4mm^2$) was added to the well with the growing cells and incubated for 72h. As control the cells without sponge and the cells with 5mM/ml $H_2O_2$ were used. After 72 hours 100 μl of cell viability PrestoBlue reagent was added to the well and incubated at 37°C for 1-3h. The active compound of cell viability assay resorufin is metabolized in viable cells to the resazurin, which has different level of absorbance. Then

the medium was used for measurement the absorbance at 560 nm. The experiment was repeated in duplicate three individual times.

## 3 Results and discussion

Fig. 2 shows the RBS spectra for the GO+ $H_2O$ suspensions poured on Si substrates, dried in air and then analysed using 1.3 MeV $H^+$ ions at the incidence angle of 60°(a) and at incidence angle 0°(b). RBS has a good depth resolution of the order of several nm, and a very good sensitivity for heavy elements, of the order of parts-per-million (ppm). The analysed depth is typically about tens microns for incident protons. Presently it was not possible to evaluate the thickness of the three solutions after drying because the distributions were not homogeneous and because of the presence of the thick silicon substrate.

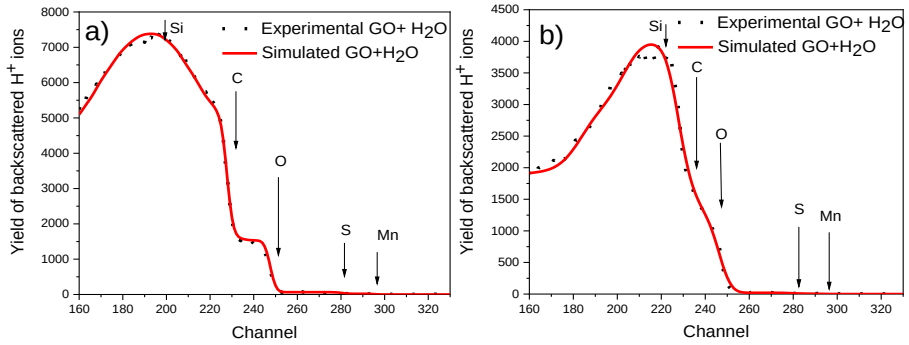


**Fig. 2.** The RBS spectra for GO+ $H_2O$ suspensions poured on Si substrates, dried in air and then analysed using $H^+$ ions at the incidence angle of 60°(a) and at the incidence angle of 0°(b).

In Figure 2b the oxygen contribution as well as the carbon one is partially masked by the overlapping of the silicon contribution. At 60° the Si signal is moved to lower energy as expected. It was observed that at the incidence angle of 60° a better discrimination of the oxygen and carbon contributions was observed as reported in Figure 2a. At the 60° incidence angle, a wide fraction of the layer of the suspensions can be investigated.

The detection of the reduction of the oxygen functional groups in GO can be validated by the fragmentation process of the graphene oxide platelets during the laser irradiation of the GO+Au+$H_2O$ suspension which is in agreement with the presented EDX analysis. Table II lists the atomic percentage of the elemental composition of the GO+$H_2O$, Au+$H_2O$, GO+Au+$H_2O$ suspensions obtained from the RBS analyses using the 1.3 MeV proton energy.

**Table II.** Elemental composition of GO+ $H_2O$, Au+ $H_2O$, GO+Au+$H_2O$ suspensions poured on silicon substrates evaluated by the RBS analysis.

| **SAMPLE** | **Elemental composition of the suspensions (at %)** | | | | | |
|---|---|---|---|---|---|---|
| | **C** | **O** | **H** | **S** | **Mn** | **Au** |
| **GO+ $H_2O$** | 49.0 | 35.0 | 15.2 | 0.3 | 0.5 | - |
| **Au+ $H_2O$** | 35.8 | 28.8 | 17.2 | - | - | 18.2 |
| **GO+ Au+ $H_2O$** | 56.2 | 25.8 | 17.0 | 0.3 | 0.5 | 0.2 |

In Table II the silicon contribution due to the substrate is missing because the evaluation is related the first superficial layers where the silicon contribution was not detected. In GO+ Au+ $H_2O$ is noted a lower Au concentration than in Au+$H_2O$ which is in agreement with the weighing of the gold target before and after the laser irradiation. The ablation rate of gold in GO is lower than in water because of the GO's greatest ability to absorb the laser radiation. The about 26.3 % reduction of the oxygen concentration going from GO+ $H_2O$ to GO+ Au+ $H_2O$ is congruent with the releasing of the oxygen functional group in GO as a consequence of the presence of Au NPs and graphene platelets fragmentation during the laser irradiation **[19]**. In GO+ Au+ $H_2O$ the concentration of gold is a quarter of that in Au+$H_2O$. The reason is the lower ablation rate in GO than in water as a consequence of the higher attenuation coefficient and absorptivity of GO to the laser than of water. The uncertainty in the evaluation of the elemental concentrations is less than 10 %.

Fig. 3 shows the SEM images with different magnifications of graphene flakes in GO+$H_2O$ a)- b), of the agglomerates of Au nanoparticles in Au +$H_2O$ c)- d) and of the structures in GO+ Au +$H_2O$ e)- f)- g).

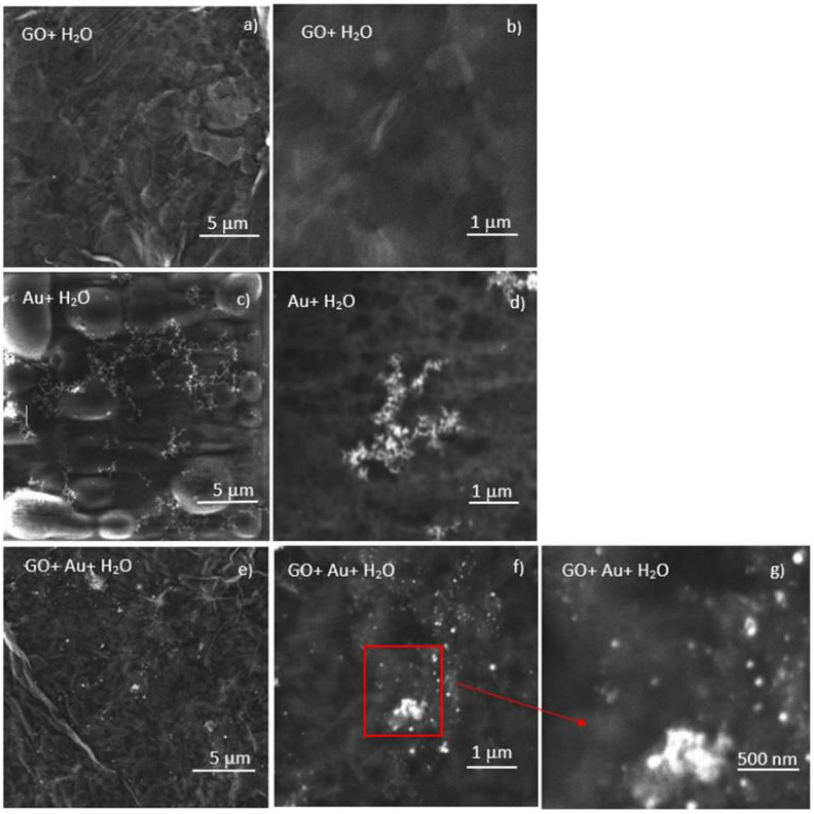


**Fig. 3.** SEM images of the GO+ Au a) b), Au+ $H_2O$ c), d) and GO+ Au+$H_2O$ e), f), g) deposited on Si substrates at magnifications of 10.4 kx, 41.5 kx and 104 kx.

The SEM view fields were 5 µm, 1 µm and 500 nm while the magnifications were 10.4 kx, 41.5 kx and 104 kx respectively. The concentration of nanoparticles, generated in Au+ $H_2O$, seems to be higher than in GO+ Au+$H_2O$ in agreement with the RBS and EDX analyses. The size of Au NPs is about 10 nm in Au+$H_2O$ while in GO+ Au+$H_2O$ the bigger size of the

structures is ascribable to Au structures anchored to the GO platelets in agreement with the AFM and SEM analyses reported in our previous work **[2]**.

Fig. 4 displays the absorbance as a function of the wavelength, evaluated for the suspensions of GO+ $H_2O$, GO+ Au+ $H_2O$ and Au+ $H_2O$ immediately after the laser irradiation and after four hours.

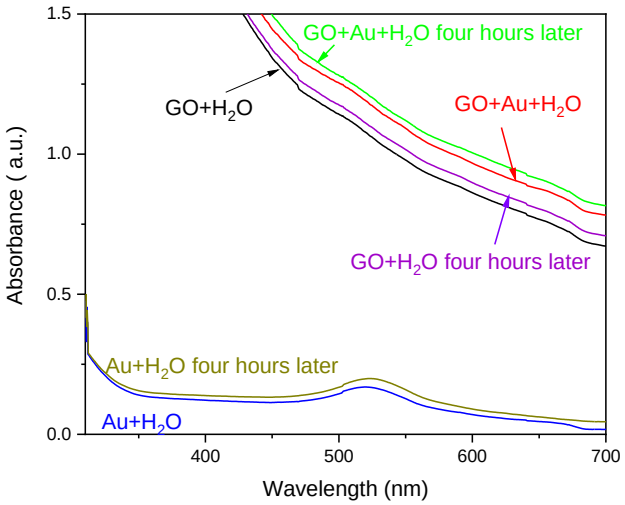


**Fig. 4.** Absorbance spectra of GO+ $H_2O$, GO+ Au+$H_2O$ and Au+ $H_2O$.

In Au+$H_2O$ after four hours of laser ablation production, the SPR (Surface Plasmon Resonance) absorption peak **[20]** around 520 nm is wider due to the Au NPs aggregation. It is in accordance with SEM analysis and assignable to the Au NPs 10 nm average size. The intensity in GO+$H_2O$ increases after four hours from the production likely because of the evaporation of the water content in the suspension. In GO+Au+$H_2O$ the SPR peak is barely visible because of the low attained Au NPs concentration and it is maintained up to four hours after the laser ablation. The intensity of the absorbance in GO+Au+$H_2O$ is higher than in GO+$H_2O$ owing to the presence of reduced GO due to the laser irradiation **[21]** as well as to the presence of Au NPs and to a higher background, due to the light scattering.

## 4 Biological considerations

The analysis of cytotoxicity of the composites was accomplished monitoring the metabolic cell culture activity as a viability indicator. The active compound of viability assay – Presto blue is resazurin which is reduced to the resorcin in metabolically active cells. The resorcin has different absorbance and fluorescence than resazurin. None of the composites was cytotoxic in any of the used cell cultures. The viability of cells with the composites was not significantly different with viability of nontreated MCF7, PC3 or rMSC cell cultures. This result is interesting for future possible applications because the materials are not cytotoxic to the cancer cell line similarly to the non-cancerous, primary mesenchymal cell line. The virgin porous PDMS was hydrophobic and this explains why it was not wettable in comparison with its two composites - GO+$H_2O$ and GO+Au+$H_2O$, in which it was modified making its composites hydrophilic. This last aspect is important in biological applications such as the peptide or protein coatings.

## 5 Conclusion

In the present paper, nanoparticles Au were synthetized by pulsed laser ablation in two different liquids. A nanosecond Nd: YAG laser was focused on the surface of a solid gold target placed either in distilled water or in distilled water containing graphene oxide. In this way two different suspensions were produced: one of Au NPs and the other of Au NPs anchored to GO nanometric platelets. Each one of the suspensions was embedded in porous PDMS sponges.

The RBS analysis showed: 1) reduction of GO during the laser ablation as a consequence of detachment of oxygen functional groups; 2) lower concentration of Au NPs in the suspension of GO+Au+$H_2O$ due to the reduction of ablation rate as a consequence of the high GO absorbance in liquid hindering the interaction between the laser and the solid target.

The production of spherical nanoparticles of about 10 nm in average diameter is indicated from the optical analysis exhibiting an absorption band centred at 520 nm as expected. A bigger size of Au NPs anchored to GO was indicated by the SEM analysis in agreement with the AFM analysis reported in our previous work. The optical analysis suggests that in the suspension containing GO the aggregation of Au NPs doesn't occur confirming the non-need for surfactant and making the suspension clean and without residue from precipitate.

The biological analysis was very positive because it revealed for all the used cells no cytotoxicity risk associated both to the use of the realized composites and the followed manufacture process.

The research has been realized at the CANAM (Center of Accelerators and Nuclear Analytical Methods) infrastructure LM 2015056 and has been supported by project GACR 19-02482S. This publication was supported by OP RDE, MEYS, Czech Republic under the project CANAM OP, CZ.02.1.01/0.0/0.0/16_013/0001812. O. J. and D. Z. acknowledge assistance provided by the Research Infrastructure NanoEnviCz (Project No. LM2018124) and the project Pro-NanoEnviCz (Reg. No. CZ.02.1.01/0.0/0.0/16_013/0001821), supported by the Ministry of Education, Youth and Sports of the Czech Republic and the European Union – European Structural and Investments Funds in the frame of the Operational Programme Research Development and Education, the ERDF/ESF project "UniQSurf - Centre of biointerfaces and hybrid functional materials" (No. CZ.02.1.01/0.0/0.0/17 _048/0007411)

## References

1. M. Cutroneo, V. Havranek V. Semian, A. Torrisi, A. Mackova, P. Malinsky, L. Silipigni, P. Slepicka, D. Fajstavr, Journal of Porous Materials **28**, 1481-1491, (2021)
2. M. Cutroneo, V. Havranek, L. Torrisi, L. Silipigni, L. Kovacik, P. Malinsky, P. Slepicka, D. Fajstavr, O. Janoušková, D. Zbořilová, A. Mackova, Vacuum **199**, 110951, (2022)
3. X. M. He, X. J. Mu, Q. Wen, Z. Y. Wen, J. Yang, C. G. Hu and H. F. Shi, Nano Res **9**, 3714-3724 (2016)
4. L. Torrisi, L. Silipigni, N. Restuccia, S. Cuzzocrea, M. Cutroneo, F. Barreca, B. Fazio, G. Di Marco, S. Guglielmino, Journal of Physics and Chemistry of Solids **119**, 62-70 (2018)
5. M. Cutroneo, V. Havranek ,A. Mackova, P. Malinsky,A. Torrisi, L. Silipigni, P. Slepicka, D. Fajstavr, L. Torrisi,et al., Surf Interface Anal., 1–9 (2021)

6. M. Cutroneo, V. Havranek, A. Mackova, P. Malinsky, L. Torrisi, L. Silipigni, B. Fazio, A. Torrisi, K. Szokolova, Z. Sofer, J. Stammers, Materials Chemistry and Physics **232**, 272-277 (2019)
7. M. Cutroneo, L. Torrisi, V. Havranek, A. Mackova, P. Malinsky, A. Torrisi, J. Stammers, Z. Sofer, L. Silipigni, B. Fazio, M. Fazio, R. Böttger, NIMB **460**, 169-174 (2019)
8. R. K. Upadhyay, N. Soin, S. S. Roy, RSC Adv. **4**, 3823–3851 (2014)
9. L. Torrisi, L. Silipigni, M. Cutroneo, A. Torrisi, Vacuum **173** 109175 (2020)
10. L. Torrisi, L. Silipigni, D. Manno, A. Serra, V. Nassisi, M. Cutroneo, A. Torrisi, Vacuum **178** 109451 (2020)
11. L. Torrisi, L. Silipigni and G. Salvato, J. of Materials Sci.: Mater. in Electronics, **31**(14) 11001-11009 (2020).
12. R. Lindley, R. Gilgenbach, C. Ching, J. Lash and G. Doll, Journal of Applied Physics **76**(9), 5457–5472 (1994)
13. G. Yang, Progress in Materials Science **52**(4), 648–698 (2007)
14. https://litron.co.uk/
15. L. Silipigni, G. Salvato, B. Fazio, G. Di Marco, E. Proverbio, M. Cutroneo, A. Torrisi, L. Torrisi, Journal of Materials Science: Materials in Electronics **32**, 8703–8715 (2021)
16. M. Mayer, SIMNRA version 6.06, Max-Planck-Institut fur Plasmaphysik Garching, Germany, 2006. http://www.rzg.mpg.de/~mam/
17. J. Ziegler, M. Ziegler and J. Biersack *NIM B* 268(11-12), 2010, 1818-1823
18. M. Cutroneo, A. Torrisi, V. Ryukhtin, M. Dopita, L. Silipigni, A. Mackova, P. Malinsky, P. Slepicka and L. Torrisi, Journal of Instrumentation **15**, 3, C03044 (2020)
19. G. Moon, Y. Park, W. Kim, and W. Choi, Carbon **49,** 11 3454–3462 (2011)
20. M.A. García, J. Phys. D: Appl. Phys. **44** (28), 283001–281/43 (2011)
21. H. Shi, C. Wang, Z. Sun, Y. Zhou, K. Jin, S. A. T. Redfern and G. Yang, Optics Express **22** (16), (2014)